Solution - Processed - ZnO - Mediated Semiconductor Bonding with High Mechanical Stability, Electrical Conductivity, Optical Transparency, and Roughness Tolerance

AUTHOR(S):

Yamashita, Tatsushi; Hirata, Soichiro; Inoue, Ryoichi; Kishibe, Kodai; Tanabe, Katsuaki

WILEY-VCH

Solution-Processed-ZnO-Mediated Semiconductor Bonding with High Mechanical Stability, Electrical Conductivity, Optical Transparency, and Roughness Tolerance

*Tatsushi Yamashita, Soichiro Hirata, Ryoichi Inoue, Kodai Kishibe, and Katsuaki Tanabe**

Department of Chemical Engineering, Kyoto University, Nishikyo, Kyoto 615–8510, Japan

E-mail: tanabe@cheme.kyoto-u.ac.jp

Keywords: semiconductors, wafer bonding, electronics, photonics, devices

Semiconductor bonding mediated by a transparent conductive oxide, ZnO, prepared by a simple solution spin-on process, is presented. The ZnO synthesis, sintering, and bonding processes are realized in a single step, thus providing a highly efficient semiconductor bonding method. The ZnO-mediated bonds simultaneously exhibit high mechanical stability, electrical conductivity, and optical transparency. The bonding's high tolerance for the roughness of the surfaces to be bonded is also demonstrated, due to the soft, deformable interfacial contact agent that is solidified in the bonding process, in contrast to direct bonding and bonding mediated by solid-state materials. Furthermore, the fabrication and operation of solar-cell devices are demonstrated using the developed ZnO-mediated bonding technique, with current paths across the bonded interfaces, thus verifying the practical applicability of the bonding scheme. The developed ZnO-mediated bonding scheme leads to a low-cost, high-performance heterostructured optoelectronic device fabrication and integration.

1. Introduction

Semiconductor wafer bonding is a skillful fabrication method used in various applications in electronics and photonics.[1–5] The bonding technique is utilized to form high-crystalline-quality homo- and heterostructures of semiconductor materials with low defect densities, which are otherwise difficult to obtain via the conventional growth methods[6–8] owing to the existence of insulating oxide interlayers or crystalline lattice mismatches. Semiconductor bonding is, therefore, promising for the fabrication of high-performance semiconductor

optoelectronics, and has been employed to generate a variety of devices such as light-emitting diodes,[9–11] lasers,[12–16] photodetectors,[17,18] and solar cells.[19–22] Nevertheless, the wafer surface condition for the conventional direct bonding and bonding mediated by solid-state materials such as oxides[3,13] or metals[9,14] is severely restricted because the surface roughness and particulates worsen the interfacial stability and conductivity. In addition, interfacial optical transparency is a crucial factor for many optoelectronic applications, including multijunction solar cells[19–22] and waveguide-integrated hybrid lasers.[12,15–17] Semiconductor wafer bonding mediated by transparent conductive oxides[23–27] is a promising alternative to mitigate such a restriction while acquiring high electrical conductivity and optical transparency. In this study, we chose ZnO, a low-cost, earth-abundant, and environmentally friendly material, in contrast to the conventional indium-oxide-based transparent conductive oxides. In this work, a spin-on, solution transparent-conductive-oxide synthesis process was employed for the formation of transparent-conductive-oxide-mediated semiconductor bonding. Such a solution-based transparent-conductive-oxide bonding approach benefits from a practical merit of having significantly higher tolerances for surface roughness and particulates, which mitigates the growth condition requirements,[28] thanks to the deformable interfacial contact agent that is solidified in the bonding process. Additionally, in our process, the ZnO synthesis, sintering, and bond formation are simultaneously carried out in a single step, and therefore provide large advantages in terms of production costs and throughputs.

2. Results and Discussion

2.1. ZnO and Bond Formation

Figure 1 shows a typical cross-sectional scanning electron microscope image of the ZnO-bonded interface (left), along with that of a directly bonded Si/Si interface with no mediating agent, bonded with the same condition as a reference (right). The wafers are thus firmly and uniformly in contact with each other with a sufficient mechanical stability to endure the

cleavage of the bonded pair sample. As seen comparing those images, only the ZnO-bonded interface is observed to have an interlayer of thin film with a thickness around 2 μm, but not for the directly bonded interface. Therefore, formation of an interlayer at the bonded semiconductor interface has been verified, which must have come from the synthetic precursor solution. Now, we analyze the synthesized thin layer to identify it as ZnO. **Figure 2** and **3** present energy-dispersive x-ray and Raman scattering spectra, respectively, from the synthesized layer. We thus detected major amounts of zinc and oxygen elements in the energy-dispersive x-ray spectrum, as observed in Figure 2. The carbon and silicon peaks in Figure 2, incidentally, can be attributed to ambient organic contaminants and the underneath Si wafer, respectively. The Raman scattering peaks seen in Figure 3 are confirmed to be at the same positions as those in the reference studying ZnO.[29] These analysis results indicate that ZnO is formed as the bonding interlayer as expected.

2.2. Optical Transparency

Figure 4 shows the optical transmission spectrum of the ZnO layer. The ultraviolet absorption below 375 nm corresponds to the ZnO bandgap, 3.3 eV, which is another confirmation of the formation of ZnO as our bonding interlayer. The ZnO layer is thus observed to have high optical transmissivity, higher than 90%, in a wide range of wavelengths. In this way, semiconductor interfaces produced by our ZnO-mediated bonding approach would have small optical losses, which is a good thing and makes our approach suitable for various optoelectronic applications, such as multijunction solar cell devices. Particularly, the transmittance is over 99% for wavelengths longer than 600 nm, whose wavelength region corresponds the transmitting rays from the top subcell to the subsequent subcells in multijunction solar cell structures.[19–22,26–28]

Let us discuss the potential optical reflection at the bonded interfaces because of the refractive-index mismatch between ZnO and semiconductor materials. ZnO is known to have refractive indices about 1.6 for optical frequencies,[30] as also demonstrated in the low reflectivity on glass in Figure 4, while typical inorganic semiconductor materials such as Si, GaAs, and InP have refractive indices about 3.5. As a rough estimate based on these representative refractive-index values, a single ZnO/semiconductor interface would have a reflectivity of 14%. Therefore, a ZnO-bonded semiconductor interface with a ZnO interlayer with a thickness sufficiently larger than the optical wavelength would have a net reflectivity of 26%. Such a degree of interfacial optical reflectance may not be preferable for a number of optoelectronic applications. However, for the interlayer thicknesses around the order of the optical wavelengths, the reflectivity varies in an oscillating manner on the interlayer thickness and the optical wavelength, and therefore, can be controlled by the ZnO thickness, depending on each application. In addition, such an interfacial reflectance could be even positively utilized, for example, for current matching in multijunction solar cells, by the reflectivity tuning by the ZnO interlayer thickness. Moreover, the reflectance can be eliminated by employing a ZnO thickness sufficiently smaller than the optical wavelength, along with an account for the trade-off with the surface-roughness tolerance. The ZnO thickness can be controlled by the choice of various parameters, including the wettability of the semiconductor surface, the organic solvent species, the spin-coating rotation velocity, and the precursor coating repetition.

2.3. Bonding Temperature and Coating Repetition

Figure 5 shows the dependence of the interfacial electrical resistivity at the bonded interface on repetition of the coating and bonding temperature. It is found that when we repeated spin-coating 5 times, reproducibility and electrical conductivity were significantly improved as compared to the case of coating only once. The interfacial electrical conductivity seemingly

becomes higher in the intermediate temperature region, but not very low or high temperatures. This electrical conductance tendency can be attributed to the following factors. The conductivity increases with the increase in bonding temperature in the lower-temperature regime because of the increase in ZnO crystalline grain sizes, leading to the decrease in the interfacial electrical resistance at the grain boundaries.[31,32] The conductivity, conversely, decreases with the increase in bonding temperature in the higher-temperature regime, presumably because of the unwanted Zn_2SiO_4 formation at the interfaces between ZnO and SiO_2.[32,33]

2.4. Surface-Roughness Tolerance

To demonstrate the versatility of our ZnO-mediated bonding scheme, we carried it out for rough semiconductor (Si in this case) surfaces. We intentionally roughened the Si wafer surface by dipping it in hydrofluoric-nitric acid etching solution, to generate rough-surface samples with root mean square roughnesses of 0.10, 0.19, and 1.23 μm. It is known that the Si etching mechanism goes as follows:

$$3Si + 4HNO_3 \rightarrow 3SiO_2 + 4NO + 2H_2O \quad (1)$$

$$SiO_2 + 6HF \rightarrow H_2SiF_6 + 2H_2O \quad (2)$$

by the oxidation of Si surface to form SiO_2 by nitric acid and subsequent dissolution of SiO_2 by hydrofluoric acid.[34] We tried the direct semiconductor bonding[19,28] with no interfacial mediating agent between the roughened Si surface and a polished smooth Si surface at 600 ºC for 3 hours, but failed and no bond was formed at all for any of the roughnesses. This failure result is necessary because the conventional direct wafer bonding method[1,19–22,28] is known not to be successful for a bonding surface roughness greater than 10 nm.[28] On the other hand, we successfully bonded the roughened surface and a polished surface by the ZnO-mediated bonding scheme at 600 ºC, for all the roughnesses. **Figure 6** and **7** show the resulted

interfacial bonding strength and current–voltage characteristics on the surface roughness. Remarkably, a mechanical strength of over 600 kPa in the bonded interface was obtained for a large surface roughness of around 100 nm. For the electrical property, the ohmic characteristics were obtained for all the roughnesses. At this stage, we are not sure about the mechanism for the difference in the electrical property on surface roughness. Although the bonded interface simply comprises a combination of two Si/ZnO interfaces in principle, some factors, such as the contacting area, may vary and provide different influences on the resulting interfacial electrical conductivities. In this way, we have experimentally demonstrated that the ZnO precursor solution mitigates the tolerance for the roughness of the surfaces to be bonded thanks to the soft, deformable bonding agent that is solidified during the bond formation after contact, verifying one of the advantages of our approach. This effect of the ZnO-mediated bonding is important for applications because in many cases bonding surfaces generally have a certain degree of roughness, since those surfaces are typically top surfaces that have undergone some fabrication procedures such as chemical treatments, crystal growth, or micro/nano processes. It is also worth noting that our experiments in this study were carried out entirely in a non-cleanroom, regular experimental room, thus also demonstrating that our ZnO-bonding scheme exhibits high particulates tolerance, in contrast to direct bonding and bonding mediated by solid-state materials.

2.5. Mechanical Stability and Electrical Conductivity Improved by Mono-Ethanolamine

For the following experiments, we set the bonding temperature at 300 °C,[5,19,28,35] accounting for the prevention of degradation of active functional semiconductor materials, including delicate micro/nanostructures such as quantum wells and dots, and for the thermal-expansion mismatch for the cases of bonding of dissimilar materials. We found that the HF surface pretreatment increases the interfacial electrical conductivity in the bonded interfaces, but the hydrogen-terminated Si surface after the HF treatment[36] has poor wettability with the ZnO-

precursor solution, which is a polar solution. Incorporation of mono-ethanolamine (MEA) is known to improve the wettability and therefore, the stability of the sol-gel-prepared ZnO films with glass[37] and Si[38] substrates, owing to the function of MEA as a surfactant. We, therefore, added MEA (0.2 mol/L, unless noted otherwise) into the ZnO-precursor solution, for the purpose of stabilizing the bonded interface for the following experiments.

For the interfacial mechanical stability in our ZnO-mediated bonding, the wafers are firmly and uniformly kept in contact with each other with a sufficient mechanical stability to endure the cleavage of the bonded pair sample, as we have been seen in Figure 1. We have also carried out peel strength tests to evaluate the bonding strengths of Si/ZnO/Si interfaces. The measured interfacial bonding strengths were 850 and 550 kPa for the bonding cases with (0.2 mol/L) and without MEA addition, respectively. These values indicate sufficiently high interfacial mechanical stabilities to endure a series of optoelectronic device manufacturing processes and user operations.

Figure 8 shows the current–voltage characteristics across the bonded interfaces prepared with and without MEA addition to the ZnO-precursor solution. As observed in the straight current–voltage curves, the ohmic electrical property was obtained for our ZnO-mediated-bonded interfaces. It should be noted that the current–voltage data in Figure 8 includes all the series resistances through the sample. We therefore independently determined the contact resistance of the metal electrode/semiconductor interfaces by the transmission line method, and then determined the nominal resistivity at the bonded interface by subtracting it from the slope of the current–voltage curve in Figure 8. We then obtained an interfacial electrical resistance of 0.048 ohm cm^2 for the case of addition of 0.2 mol/L MEA. Such a high interfacial electrical conductance value is thought to be highly preferable for most optoelectronic device applications such as solar cells.[26,39] Incidentally, the interfacial

resistivity value we obtained is comparable or even lower than the values for indium-tin-oxide-mediated semiconductor wafer bonding.[26,27] In this way, we found that the addition of MEA enhances the interfacial electrical conductivity in the bonded interface. In addition to the abovementioned surfactant effect of MEA, improved crystallinity in the ZnO film, caused by slower ZnO crystal growth in the heating in the bonding process, owing to the increase in the boiling temperature of the ZnO-precursor solution by the addition of MEA,[40–42] might have also contributed to the increase of electrical conductivity. Addition of more MEA, however, caused an increase in interfacial electrical conductivity, resulting in 0.13 ohm cm^2 for 0.4 mol/L and 0.40 ohm cm^2 for 1.25 mol/L. This resultant tendency can be attributed to the effect of the excess addition of MEA to cause a decrease in electrical conductivity due to its own insulating property. Therefore, it is important to recognize that there is an optimum amount of MEA to be added to the ZnO-precursor solution to obtain the highest electrical conductivity at the bonded semiconductor interface. If one needs further interfacial conductivity for some cases, doping of Al into ZnO, for example, by adding $Al(NO_3)_3$ to the ZnO-precursor solution, may effectively work to lower the resistance.[43–47]

2.6. Doping-Polarity Dependence

So far, we have carried out the bonding experiments only for the combination of *p*-type Si/*p*-type Si. **Figure 9** shows the current–voltage characteristics of the bonded interfaces with other doping-polarity (*p*-type or *n*-type) combinations. For the *n*-type Si wafers, we used the same specifications as for the *p*-type wafers: single side polished, thickness: 280 μm, crystalline plane orientation: <100>, dopant: phosphorus, doping concentration: ~ 1×10^{19} cm^{-3}. Together with the result in Figure 8, we obtained ohmic interfacial electrical characteristics at the bonded interfaces for all of the doping-polarity combinations. Thus, we have demonstrated that our bonding scheme can flexibly deal with the bonding of any kind of doping-polarity combination of semiconductor materials. It is worth noting that the addition

of MEA to the ZnO-precursor solution enhanced the interfacial electrical conductivity for all of the doping-polarity combinations.

2.7. Device Fabrication and Operation Demonstration

Using the ZnO-mediated bonding technique, we fabricated Si solar cells bonded to Si wafers to demonstrate the applicability of our bonded semiconductor interface in optoelectronic devices. Si solar cells were prepared by thermal diffusion of phosphorus (10^{19}–10^{20} cm^{-3}) into one side of the surface region of a double-side-polished epi-ready *p*-type Si <100> wafer doped with boron (doping concentration of ~ 1×10^{16} cm^{-3}). After the thermal diffusion of phosphorus, the boron doping concentration on the other surface was increased to a level of 10^{19}–10^{20} cm^{-3} by ion implantation in order to provide a sufficient electrical conductance at the bonded interface. The *p*-type side of the Si solar cell wafer was bonded to a bare Si wafer (the same *p*-type Si wafer used for the above bonding investigations) mediated by ZnO under the same process conditions as those in the bonding investigation. A front grid contact on top of the Si cell and a bottom contact on the back of the bare Si wafer were formed with the Au/Au–Ge–Ni material in the same manner as in the bonding investigation. It should be noted that, in this electrode configuration, the current passes through the bonded interface in the solar cell operation. Therefore, these solar cell fabrication and operation tests are suitable to evaluate the validity of our bonding scheme for optoelectronic device applications. For comparison, we also prepared a pristine reference solar cell sample from the same Si solar cell wafer with the same top and bottom electrodes but standing alone, not bonded with a bare Si wafer. Through this performance comparison, the loss in the power conversion efficiency by the electrical resistance at the bonded interface can be estimated.

Figure 10 shows the light current–voltage characteristics of the best bonded and best reference cells under AM1.5 G, 1-sun (100 mW cm^{-2}) illumination. The performance of the

bonded cell was a little lower than that of the reference cell (e.g., the energy-conversion efficiencies of the bonded and reference cells were 6.54% and 8.00%, respectively). However, our fabricated cells had relatively large statistical fluctuations in their performances, and the average energy-conversion efficiency values of the bonded and reference cells were 6.12% and 6.18%, respectively; the performances of the bonded cells were highly comparable to those of the unbonded reference cells. Therefore, the bonding process and the bonded interface did not degrade the solar cell and its performance, and thus our bonding scheme is suitable for optoelectronic device applications.

2.8. Heterostructure Formation

An advantage of the wafer bonding method over the conventional epitaxial growth method is the applicability for lattice-mismatched systems. Here, we demonstrate our ZnO-mediated bonding scheme to fabricate an InP/Si heterostructure, whose lattice mismatch is as large as 8%. We bonded the Si wafer piece to a *n*-type InP wafer piece doped with sulfur with a doping concentration of ~1×10^{19} cm^{-3} in a similar manner as above, but without the addition of MEA for no particular reason. **Figure 11** shows the current–voltage characteristics across the InP/Si interfaces prepared by the ZnO-mediated bonding, and direct bonding[19,28] with similar process conditions as the ZnO-mediated bonding (0.1 MPaG, 300 ºC, 3 h bonding, after HF surface pretreatment, but without ZnO-precursor solution application) as a reference. Incidentally, it should be noted that the electrical resistivity seen in the current–voltage plot here is dominated by the measurement setup circuit but not the specimen because for these samples, the resistivities at the bonded interfaces as well as the other partial resistivities in the samples are relatively small, and therefore, the similarity of the current-voltage curves does not necessarily represent the similarity in the electrical characteristics of the bonded interfaces between these samples. As observed in Figure 11, in this way, an ohmic, low-resistivity InP/Si heterostructure was formed by the ZnO-mediated bonding scheme. Such III-V

compound semiconductor / Si bonded heterostructures have been thought to be promising for high-performance optoelectronics,[6–8,12–17,22,27,28,35] by combining each materials advantageous characteristics, including high carrier mobility and optical radiation efficiency of compound semiconductors, and low cost, earth abundance, light weight, and high thermal conductivity of Si.

3. Conclusion

In this work, solution-processed transparent conductive oxide-mediated semiconductor bonding was proposed and experimentally demonstrated, as a concept to provide a useful and high-performance bond formation method. We employed ZnO as the transparent conductive bonding agent, motivated by its low cost, earth-abundance, and environmental friendliness. High mechanical stability, electrical conductivity, optical transparency, surface-roughness and particulate tolerances were simultaneously acquired in our ZnO-bonded semiconductor interfaces. Importantly, we carried out the ZnO synthesis, sintering, and bonding processes in a single step, realizing a highly efficient semiconductor bonding scheme. Furthermore, we demonstrated fabrication and operation of solar cells using the developed bonding technique, with current paths across the bonded interfaces, thus verifying the validity of our scheme for practical applications. Our solution-processed-ZnO-mediated bonding scheme will be useful for flexible optoelectronic materials integration, leading to low-cost production of high-performance electronic and photonic devices.

4. Experimental Section

Sample Preparation: We conducted all the experimental processes in this study in a non-cleanroom, regular experimental room with a particle density around 5 million m^{-3}, which we measured with a regular particle counter. As a precursor for ZnO, 1 g of $Zn(CH_3COO)_2 \cdot 2H_2O$ was dissolved in a solvent of 10-ml ethanol, with an addition of ca. 7.5-ml 28% NH_3 aq to

attain a pH of 10.[48] In this process of preparing the solution, CH_3COONH_4 is generated by the reaction:[42,48]

$$Zn(CH_3COO)_2 + 2NH_3 + 2H_2O \rightarrow Zn(OH)_2 + 2CH_3COONH_4. \quad (3)$$

We used single-side-polished *p*-type Si wafers (thickness: 280 μm, crystalline plane orientation: <100>, dopant: boron, doping concentration: ~ 1×10^{19} cm^{-3}) for most experiments in this study, unless noted otherwise. The surfaces of the polished sides of the Si wafers were coated with a photoresist film to protect the Si surface from scratches and particulates during the process of being diced into ~1 cm^2 pieces. The diced wafers were submerged in acetone for 5 min to remove the photoresist film. The Si pieces then underwent a wet HF treatment (10% aq, 1 min) to remove the native oxide layer on the Si surfaces.[35,49] The aqueous ZnO precursor was then spin-coated onto the polished-side surface of a Si piece at 3000 rpm for 30 s. This spin-coating process was repeated 5 times in order to acquire higher mechanical stability in the bonded interfaces and reproducibility in the experimental measurement results. The ZnO-coated Si piece was then bonded to the surface of the polished side of a bare Si piece under a uniaxial pressure of 0.1 MPaG at 300 ºC for 3 hours. In this bonding process, ZnO is synthesized at the semiconductor interface, due to the heating, simultaneously with the bond formation, by the reaction:[42,48]

$$Zn(OH)_2 \rightarrow ZnO + H_2O. \quad (4)$$

Characterization: Detaching normal stresses were measured for the bonded samples to represent the bonded interfacial mechanical strength. It is worth mentioning that in our preparatory experiments, each of the HF treatment before bonding, and the pressure application in bonding, was found to result in a significantly higher interfacial mechanical strength and electrical conductivity in the bonded interface than the case of its corresponding

reference run without it, and therefore, we employed them in our experiments. For electrical measurements, metal electrodes comprising an Au–Ge–Ni alloy (80:10:10 wt%) and pure Au with thicknesses of 30 and 150 nm, respectively, were sequentially deposited to both of the outer sides of the bonded Si pieces by thermal evaporation. Then we measured the current–voltage characteristics across the bonded interfaces. For energy-dispersive x-ray spectroscopy and Raman scattering spectroscopy measurements, ZnO-coated Si wafers were also prepared in the same way as above, i.e., annealed at 300 ºC after spin-coating to mimic the bonding condition. For optical transmission measurements, ZnO-coated glasses, instead of the Si wafers, were also prepared, in the same way as above, i.e., annealed at 300 ºC.

Acknowledgements

This study was supported, in part, by the Japan Society for the Promotion of Science (JSPS) and the Nanotechnology Platform Project sponsored by the Ministry of Education, Culture, Sports, Science and Technology (MEXT), Japan.

Received: ((will be filled in by the editorial staff))
Revised: ((will be filled in by the editorial staff))
Published online: ((will be filled in by the editorial staff))

References

[1] Q. Tong, U. M. Goesele, *Adv. Mater.* **1999**, *11*, 1409.

[2] S. Noda, K. Tomoda, N. Yamamoto, A. Chutinan, *Science* **2000**, *289*, 604.

[3] G. K. Celler, S. Cristoloveanu, *J. Appl. Phys.* **2003**, *93*, 4955.

[4] M. Madsen, K. Takei, R. Kapadia, H. Fang, H. Ko, T. Takahashi, A. C. Ford, M. H. Lee, A. Javey, *Adv. Mater.* **2011**, *23*, 3115.

[5] T. Naito, K. Tanabe, *Nanomater.* **2018**, *8*, 1048.

[6] H. Kroemer, T. Y. Liu, P. M. Petroff, *J. Cryst. Growth* **1989**, *95*, 96.

[7] M. Sugo, Y. Takanashi, M. M. Al-Jassim, M. Yamaguchi, *J. Appl. Phys.* **1990**, *68*, 540.

[8] J. Z. Li, J. Bai, J. S. Park, B. Adekore, K. Fox, M. Carroll, A. Lochtefeld, Z. Shellenbarger, *Appl. Phys. Lett.* **2007**, *91*, 021114.

[9] W. S. Wong, T. Sands, N. W. Cheung, M. Kneissl, D. P. Bour, P. Mei, L. T. Romano, N. M. Johnson, *Appl. Phys. Lett.* **2000**, *77*, 2822.

[10] J. Chun, K. J. Lee, Y. C. Leem, W. M. Kang, T. Jeong, J. H. Baek, H. J. Lee, B. J. Kim, S. J. Park, *ACS Appl. Mater. Interfaces* **2014**, *6*, 19482.

[11] C. M. Kang, J. Y. Lee, D. J. Kong, J. P. Shim, S. Kim, S. H. Mun, S. Y. Choi, M. D. Park, J. Kim, D. S. Lee, *ACS Photon.* **2018**, *5*, 4413.

[12] J. Van Campenhout, P. Rojo-Romeo, P. Regreny, C. Seassal, D. Van Thourhout, S. Verstuyft, L. Di Cioccio, J. M. Fedeli, C. Lagahe, R. Baets, *Opt. Express* **2007**, *15*, 6744.

[13] K. Tanabe, M. Nomura, D. Guimard, S. Iwamoto, Y. Arakawa, *Opt. Express* **2009**, *17*, 7036.

[14] S. Palit, J. Kirch, G. Tsvid, L. Mawst, T. Kuech, N. M. Jokerst, *Opt. Lett.* **2009**, *34*, 2802.

[15] D. Liang, X. Huang, G. Kurczveil, M. Fiorentino, R. G. Beausoleil, *Nature Photon.* **2016**, *10*, 719.

[16] G. Crosnier, D. Sanchez, S. Bouchoule, P. Monnier, G. Beaudoin, I. Sagnes, R. Raj, F. Raineri, *Nature Photon.* **2017**, *11*, 297.

[17] H. Park, A. W. Fang, R. Jones, O. Cohen, O. Raday, M. N. Sysak, M. J. Paniccia, J. E. Bowers, *Opt. Express* **2007**, *15*, 6044.

[18] L. Chen, P. Dong, M. Lipson, *Opt. Express* **2008**, *16*, 11513.

[19] K. Tanabe, A. Fontcuberta i Morral, H. A. Atwater, D. J. Aiken, M. W. Wanlass, *Appl. Phys. Lett.* **2006**, *89*, 102106.

[20] F. Dimroth, M. Grave, P. Beutel, U. Fiedeler, C. Karcher, T. N. D. Tibbits, E. Oliva, G. Siefer, M. Schachtner, A. Wekkeli, A. W. Bett, R. Krause, M. Piccin, N. Blanc, C. Drazek, E.

Guiot, B. Ghyselen, T. Salvetat, A. Tauzin, T. Signamarcheix, A. Dobrich, T. Hannappel, K. Schwarzburg, *Prog. Photovolt.* **2014**, *22*, 227.

[21] P. T. Chiu, D. C. Law, R. L. Woo, S. B. Singer, D. Bhusari, W. D. Hong, A. Zakaria, J. Boisvert, S. Mesropian, R. R. King, N. H. Karam, *IEEE J. Photovolt.* **2014**, *4*, 493.

[22] S. Essig, C. Allebé, T. Remo, J. F. Geisz, M. A. Steiner, K. Horowitz, L. Barraud, J. S. Ward, M. Schnabel, A. Descoeudres, D. L. Young, M. Woodhouse, M. Despeisse, C. Ballif, A. Tamboli, *Nature Ener.* **2017**, *2*, 17144.

[23] P. Liu, C. Hou, Y. Wu, *Thin Solid Films* **2005**, *478*, 280.

[24] T. Hong, Y. P. Li, W. X. Chen, G. Z. Ran, G. G. Qin, H. L. Zhu, S. Liang, Y. Wang, J. Q. Pan, W. Wang, *IEEE Photon. Technol. Lett.* **2012**, *24*, 712.

[25] X. Huang, Y. Gao, X. Xu, *Opt. Express* **2014**, *22*, 14285.

[26] S. Yoshidomi, J. Fukukawa, M. Hasumi, T. Sameshima, *Ener. Proc.* **2014**, *60*, 116.

[27] N. Shigekawa, T. Hara, T. Ogawa, J. Liang, T. Kamioka, K. Araki, M. Yamaguchi, *IEEE J. Photovolt.* **2018**, *8*, 879.

[28] K. Tanabe, K. Watanabe, Y. Arakawa, *Sci. Rep.* **2012**, *2*, 349.

[29] D. Das, P. Mondal, *RSC Adv.* **2014**, *4*, 35735.

[30] C. Stelling, C. R. Singh, M. Karg, T. A. F. König, M. Thelakkat, M. Retsch, *Sci. Rep.* **2017**, *7*, 42530.

[31] Y. Natsume, H. Sakata, *Thin Solid Films* **2000**, *372*, 30.

[32] A. B. Yadav, K. Singh, A. Pandey, S. Jit, *Superlat. Microstr.* **2014**, *71*, 250.

[33] A. Barhoum, G. V. Assche, H. Rahier, M. Fleisch, S. Bals, M. P. Delplancked, F. Leroux, D. Bahnemann, *Mater. Des.* **2017**, *119*, 270.

[34] M. Steinert, J. Acker, S. Oswald, K. Wetzig, *J. Phys. Chem. C* **2007**, *111*, 2133.

[35] A. W. Fang, H. Park, O. Cohen, R. Jones, M. J. Paniccia, J. E. Bowers, *Opt. Express* **2006**, *14*, 9203.

[36] G. S. Higashi, Y. J. Chabal, G. W. Trucks, K. Raghavachari, *Appl. Phys. Lett.* **1990**, *56*, 656.

[37] V. Musat, A. M. Rego, R. Monteiro, E. Fortunato, *Thin Solid Films* **2008**, *516*, 1512.

[38] J. Lu, K. Huang, X. Chen, J. Zhu, F. Meng, X. Song, Z. Sun, *Appl. Surf. Sci.* **2010**, *256*, 4720.

[39] P. R. Sharps, M. L. Timmons, J. S. Hills, J. L. Gray, *Proc. 26th IEEE Photovolt. Specialists Conf.*, IEEE, New York, USA **1997**, 895.

[40] M. Ohyama, H. Kozuta, T. Yoko, S. Sakka, *J. Ceram. Soc. Jpn.* **1996**, *104*, 296.

[41] L. Znaidi, G. J. A. A. Soler Illia, S. Benyahia, C. Sanchez, A. V. Kanaev, *Thin Solid Films* **2003**, *428*, 257.

[42] L. Znaidi, *Mater. Sci. Eng. B* **2010**, *174*, 18.

[43] T. Minami, H. Nanto, S. Takata, *Jpn. J. Appl. Phys.* **1984**, *23*, 280.

[44] A. E. Jiménez-González, J. A. S. Urueta, R. Suárez-Parra, *J. Cryst. Growth* **1998**, *192*, 430.

[45] K. Yoshino, M. Shinmiya, N. Kamiya, J. Kosaka, M. Oshima, Y. Takamoto, K. Toyota, K. Inaba, K. Haga, K. Tokudome, *Jpn. J. Appl. Phys.* **2011**, *50*, 108001.

[46] M. Wang, W. Liang, Y. Yang, J. Yang, X. Cheng, S. H. Hahn, E. J. Kim, *Mater. Chem. Phys.* **2012**, *134*, 845.

[47] S. H. Sabeeh, R. H. Jassam, *Results Phys.* **2018**, *10*, 212.

[48] M. Smirnov, C. Baban, G. I. Rusu, *Appl. Surf. Sci.* **2010**, *256*, 2405.

[49] D. Kikuchi, S. Adachi, *Mater. Sci. Eng. B* **2000**, *76*, 133.

FIGURES

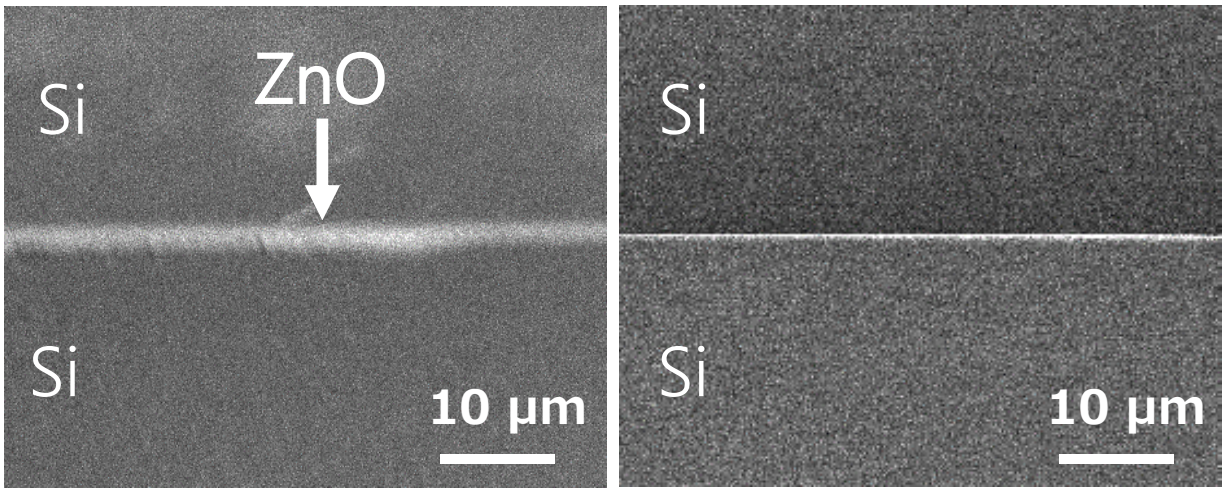

Figure 1. Cross-sectional scanning electron microscope images of (left) the ZnO-bonded interface and (right) a reference direct-bonded Si/Si interface.

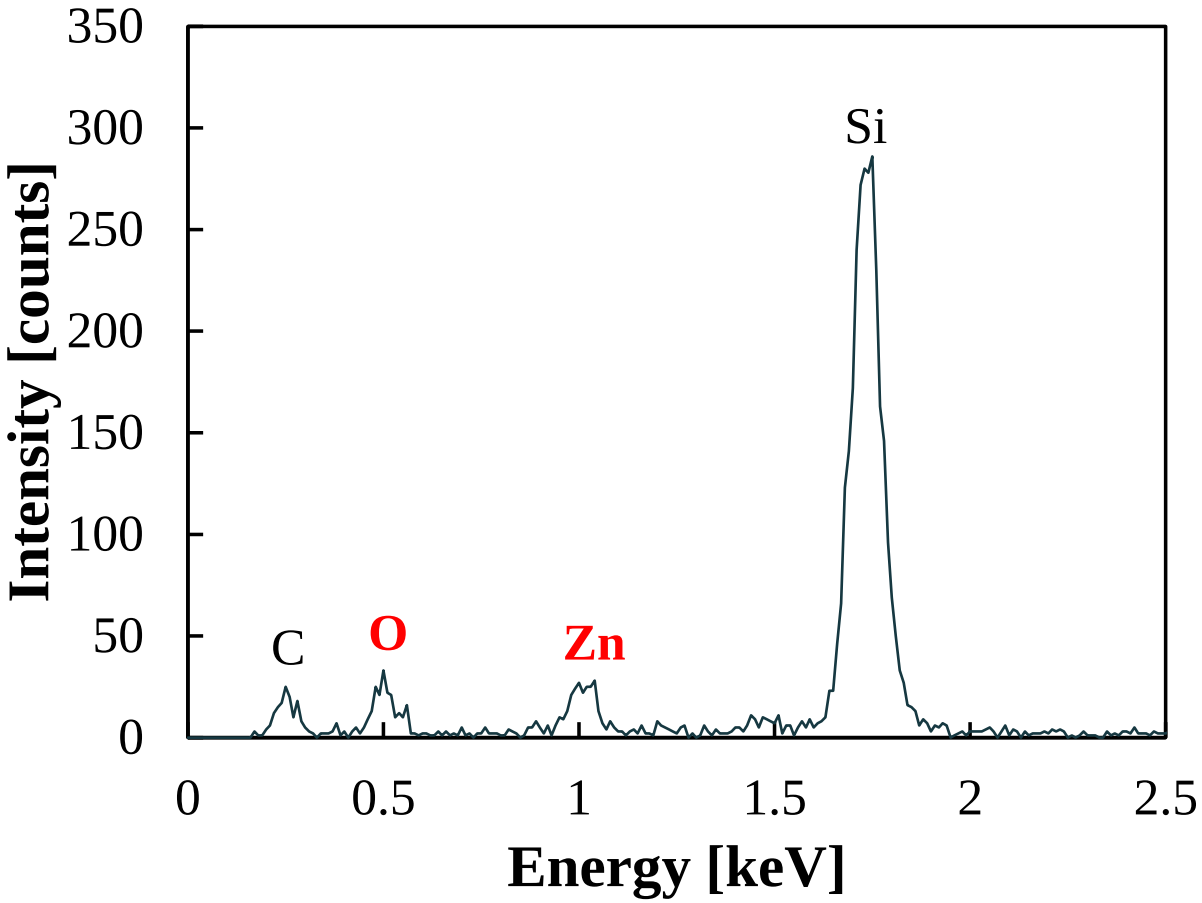

Figure 2. Energy-dispersive x-ray spectrum from the ZnO layer.

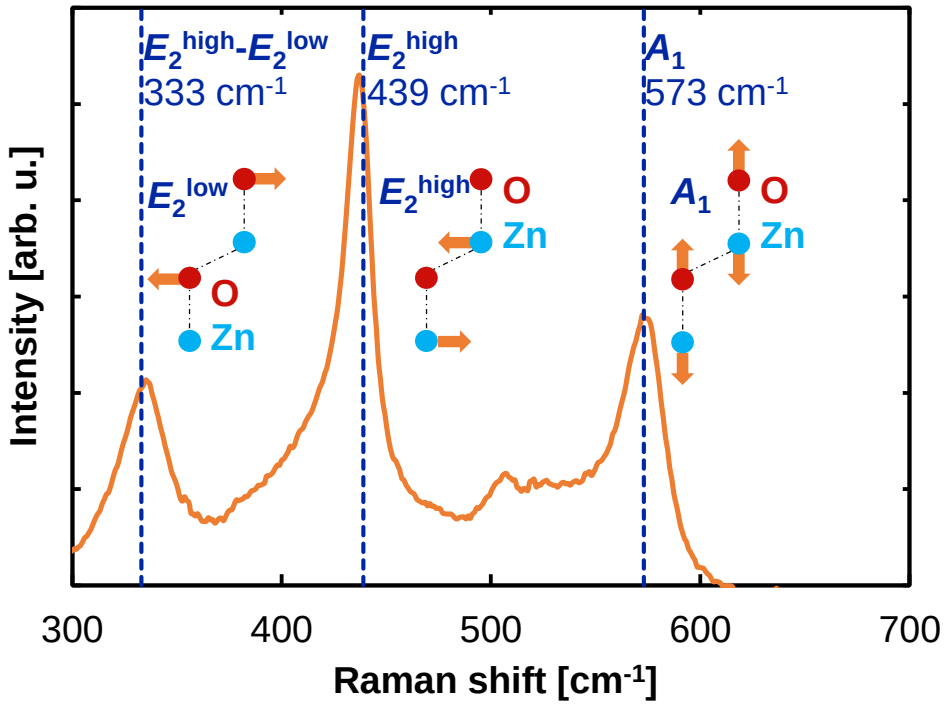

Figure 3. Raman scattering spectrum from the ZnO layer with schematics of the corresponding optical phonon modes in wurtzite ZnO.

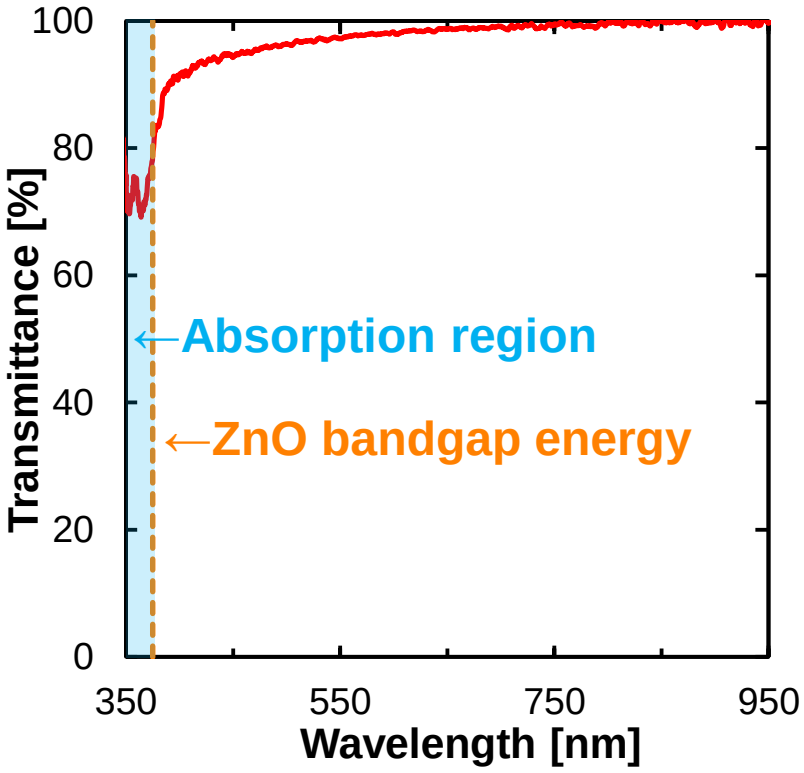

Figure 4. Optical transmission spectrum of the ZnO layer.

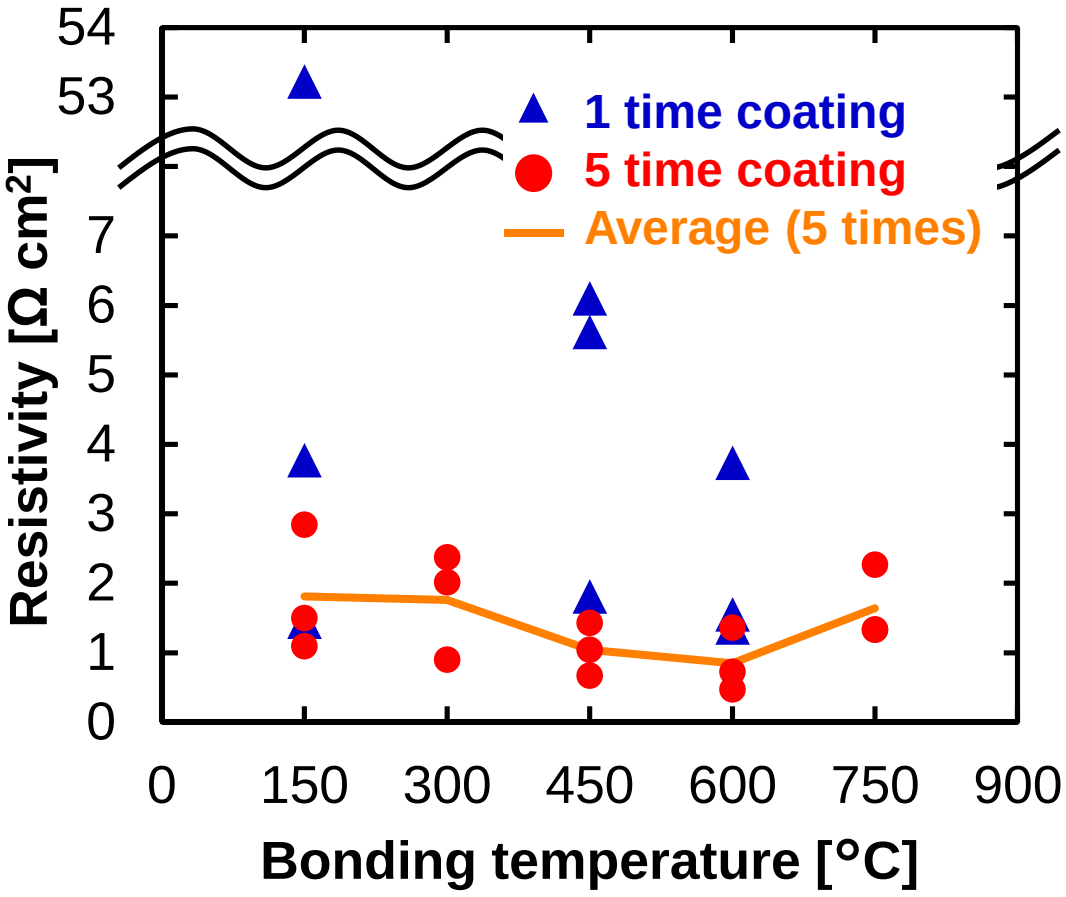

Figure 5. Dependence of the interfacial resistivity in the bonded samples on bonding temperature and coating repetition.

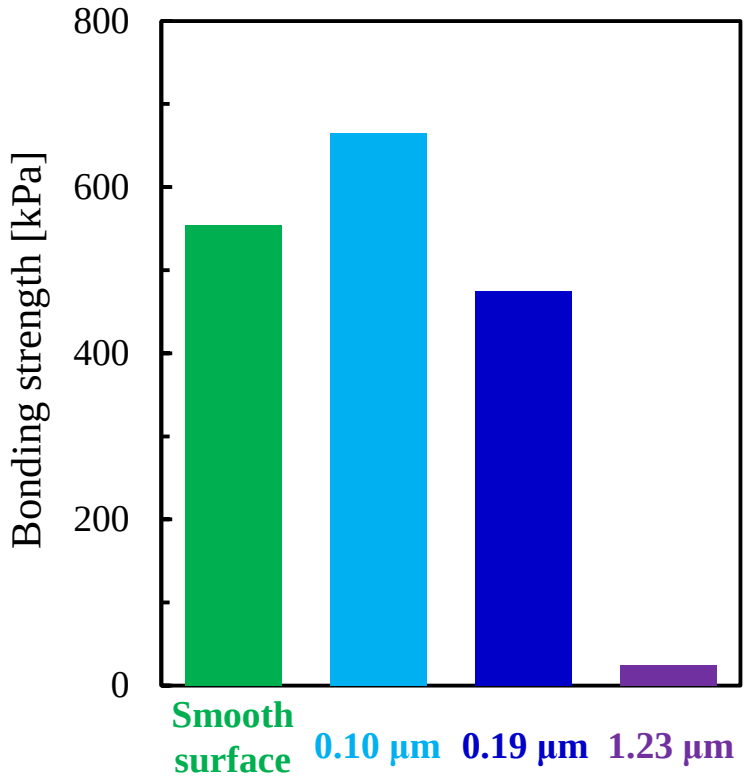

Figure 6. Interfacial mechanical strength of the bonded interfaces with smooth and roughened bonding surfaces. The numbers in µm indicate the RMS roughness.

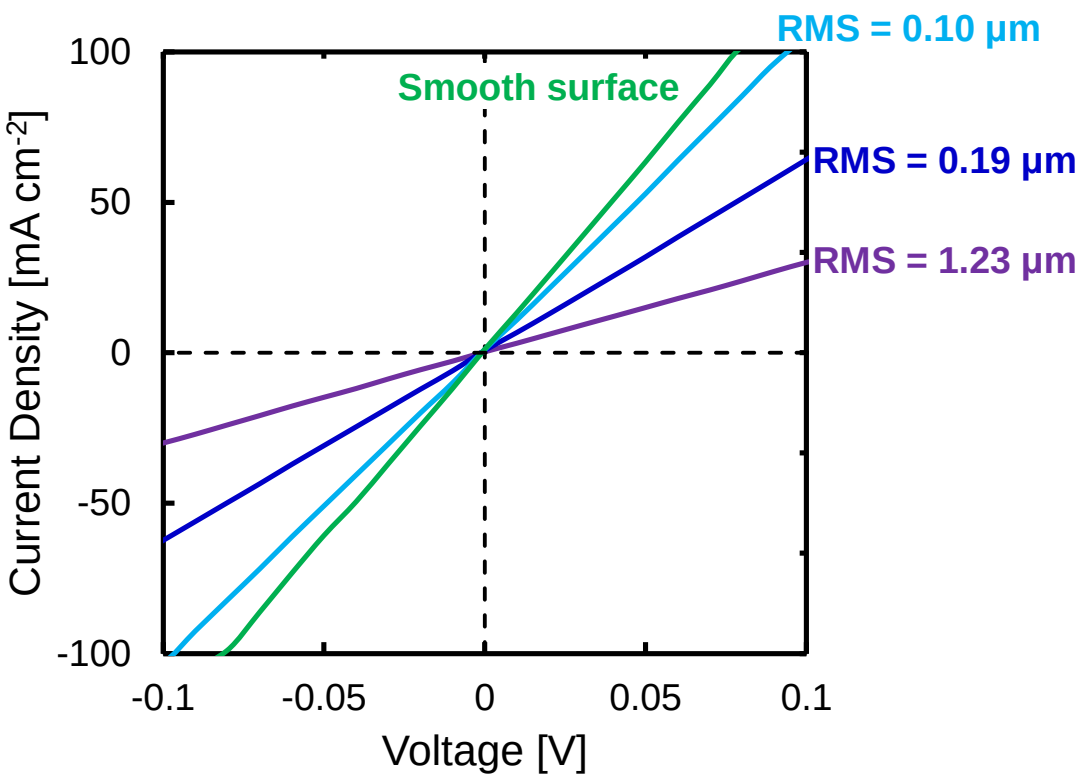

Figure 7. Current–voltage characteristics of the bonded interfaces with smooth and roughened bonding surfaces.

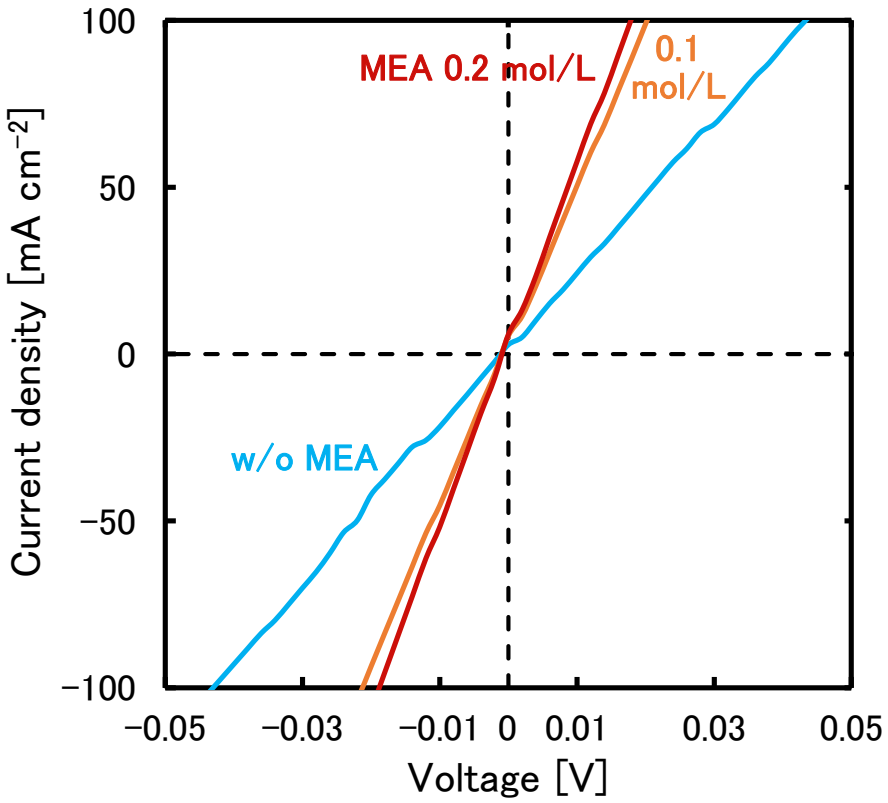

Figure 8. Current–voltage characteristics of the bonded interfaces on the amount of MEA addition.

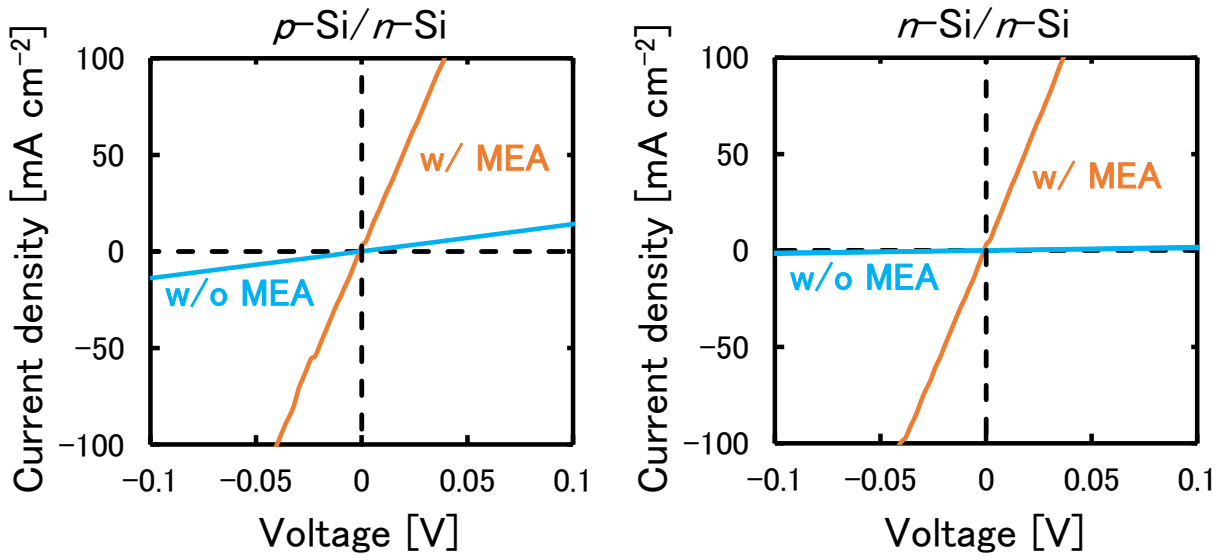

Figure 9. Current–voltage characteristics of the bonded interfaces with doping-polarity combinations of *p*-type Si/*n*-type Si and *n*-type Si/*n*-type Si.

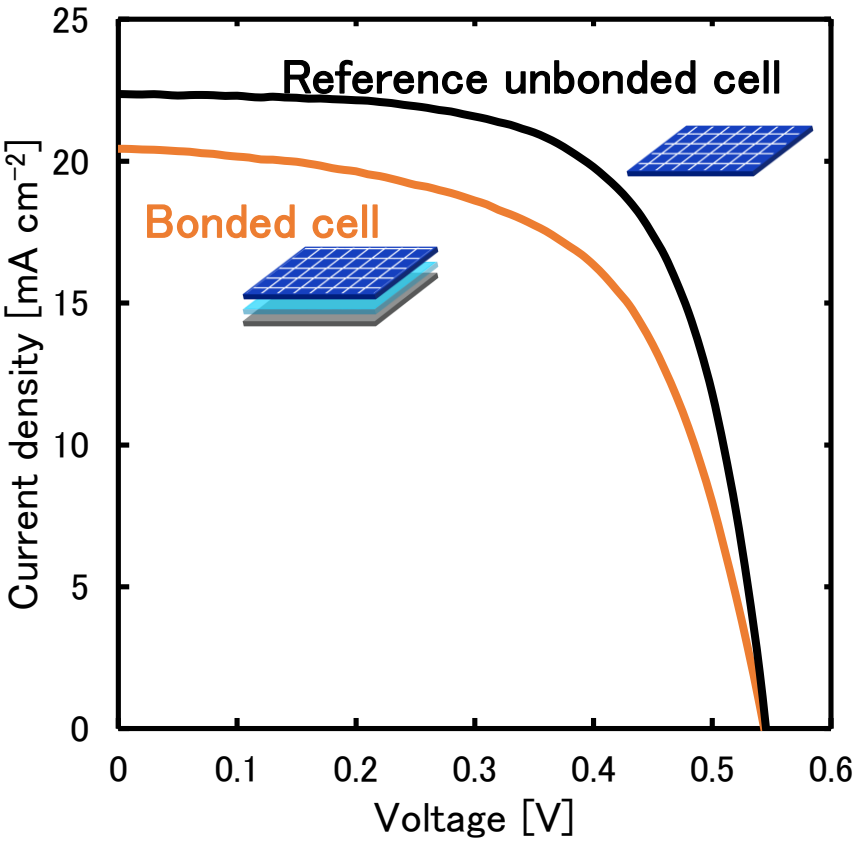

Figure 10. Light current–voltage characteristics of the best-efficiency bonded and reference unbonded Si solar cells under the AM1.5 G, 1-sun illumination.

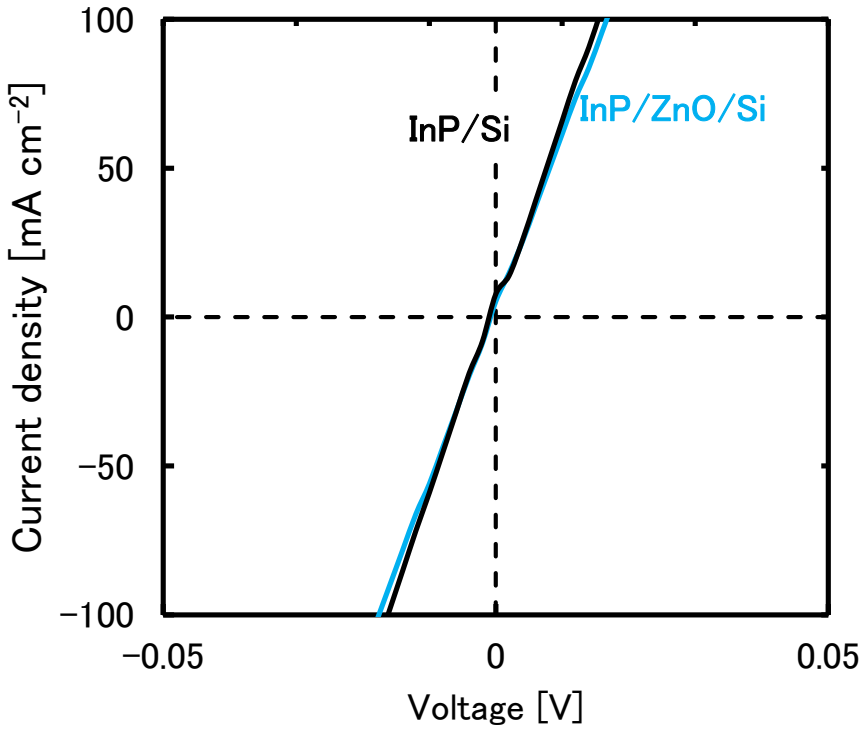

Figure 11. Current–voltage characteristics of the InP/Si interfaces prepared by the ZnO-mediated bonding and direct bonding.

The table of contents entry should be 50–60 words long and should be written in the present tense and impersonal style (i.e., avoid we). The text should be different from the abstract text.

Keyword
Transparent-conductive-oxide-mediated semiconductor wafer bonding

T. Yamashita, S. Hirata, R. Inoue, K. Kishibe, K. Tanabe*

Title
Solution-Processed-ZnO-Mediated Semiconductor Bonding with High Mechanical Stability, Electrical Conductivity, Optical Transparency, and Roughness Tolerance

Semiconductor bonding mediated by a transparent conductive oxide, ZnO, prepared by a simple solution spin-on process, is presented. The ZnO synthesis, sintering, and bonding processes are realized in a single step, thus providing a highly efficient semiconductor bonding method. The ZnO-mediated bonds simultaneously exhibit high mechanical stability, electrical conductivity, optical transparency, and roughness tolerance.

ToC figure